Published in final edited form as:

Biomaterials. 2016 January ; 74: 77–88. doi:10.1016/j.biomaterials.2015.09.032.

Co-fabrication of chitosan and epoxy photoresist to form microwell arrays with permeable hydrogel bottoms

Douglas M. Ornoff[a,b], **Yuli Wang**[c], **Angela Proctor**[c], **Akash S. Shah**[c], and **Nancy L. Allbritton**[a,c,d,*]

[a]Department of Pharmacology, University of North Carolina, Chapel Hill, NC 27599

[b]Department of Medicine, University of North Carolina, Chapel Hill, NC 27599

[c]Department of Chemistry, University of North Carolina, Chapel Hill, NC 27599

[d]Department of Biomedical Engineering, University of North Carolina, Chapel Hill, NC 27599 and North Carolina State University, Raleigh, NC 27695

Abstract

Microfabrication technology offers the potential to create biological platforms with customizable patterns and surface chemistries, allowing precise control over the biochemical microenvironment to which a cell or group of cells is exposed. However, most microfabricated platforms grow cells on impermeable surfaces. This report describes the co-fabrication of a micropatterned epoxy photoresist film with a chitosan film to create a freestanding array of permeable, hydrogel-bottomed microwells. These films possess optical properties ideal for microscopy applications, and the chitosan layers are semi-permeable with a molecular exclusion of 9.9 ± 2.1 kDa. By seeding cells into the microwells, overlaying inert mineral oil, and supplying media via the bottom surface, this hybrid film permits cells to be physically isolated from one another but maintained in culture for at least 4 days. Arrays co-fabricated using these materials reduce both large-molecular-weight biochemical crosstalk between cells and mixing of different clonal populations, and will enable high-throughput studies of cellular heterogeneity with increased ability to customize dynamic interrogations compared to materials in currently available technologies.

1. Introduction

Microfabricated platforms allow the study of biological systems with unparalleled control of the physical and chemical microenvironment to which a cell or group of cells is exposed. Such technology permits precise customization of the shape, size, and surface chemistry of the area used for cell growth [1-4]. By achieving such control, researchers gain the ability to interrogate the mechanisms and regulation of fundamental cellular processes and to create novel bio-inspired platforms [5-9]. To date, numerous types of microscale platforms have

*Corresponding author. Department of Biomedical Engineering, University of North Carolina, Chapel Hill, NC 27599, USA. Tel.: +1 919 966 2291; fax: +1 919 962 2388. nlallbri@unc.edu (N. L. Allbritton).

been developed for the high-throughput analysis of cells, but several limitations to these technologies exist. Droplet microfluidics can rapidly assay large numbers of isolated cells, but long-term culture of cells in droplets is difficult due to reduced delivery of oxygen and nutrients [10-11]. In addition, analytical reagents must be pre-loaded into the droplet with the cells and analyses subsequent to the initial screening are technically difficult to set up [12]. Micropallet or microraft arrays, consisting of a large number of individual pedestal elements, can be used as substrates on which cells can be grown. However, biochemical crosstalk (in the form of secreted paracrine signaling molecules distributed by the culture medium) and cell migration from one pedestal to another can lead to confounded data and mixing of clonal cell populations [11, 13]. Additionally, such platforms can be problematic for nonadherent cells [11, 14-15]. Microwell arrays can be used to array cells at low density into physically separate wells. However, confounding biochemical crosstalk and intermixing of clonal cell populations can nonetheless pose a problem for these platforms as well, since maintenance of cells beyond several hours necessitates that cells be exposed to a relatively large common media reservoir. While certain techniques, such as overlaying a physical barrier onto microwells seeded with cells, can reduce biochemical crosstalk and cell migration, cell survival and viability can be compromised over the long term as cells quickly consume the small quantities of culture media with which they are seeded, a consequence of the solid, impermeable substrates, such as PDMS or glass, upon which microwell arrays are generally fabricated [16].

Therefore, a platform that allows for user-customized interrogation of discrete numbers of cells, isolated so as to ensure the independence of measured responses, and yet still arrayed in a fashion that permits high-throughput study, would be a useful tool for cellular analyses. Our lab recently developed and characterized freestanding photoresist films [17]. Given the ease with which such films could be micropatterned, we sought to combine this approach with a hydrogel-based support that would yield arrays of microscale wells, each with a permeable bottom.

Chitosan is a cationic polysaccharide derived from chitin that has begun to see increased use in a number of biologically-relevant applications [18-21]. Many of the chemical and physical properties of chitosan have been well characterized [22-32]. Chitosan has been shown to be biocompatible to a number of cell types, including endothelial, hepatic, bone, and peripheral nerve cells [33-37]. Chitosan can be manipulated to form hydrogels, porous scaffolds, and dry films [21, 30, 38]. Studies have shown that capsules and films prepared from chitosan are permeable at the microscale and may have a potential role in drug and gene delivery systems [39-43]. A key feature of chitosan is the free amine group in its molecular structure, which protonates in a pH-dependent manner and induces swelling of the chitosan matrix and an increase in its network pore size. In addition to being responsible for chitosan's pH-dependent solubility, the amine group also allows the conjugation of exogenous molecules to the polysaccharide chain [20, 44-45]. Recently several research groups have devised strategies to pattern chitosan at the microscale, including on surfaces for bioreactor applications and as a semi-permeable microscaffold in a microfluidic device for the study of bacterial biofilms [20, 44, 46-47]. Due to its biocompatibility, pH-dependent solubility, and demonstrated use in certain microscale platforms, chitosan presented potential.

This report describes the co-fabrication of the biocompatible materials chitosan and 1002F epoxy photoresist to create a freestanding, two-layer hybrid film of permeable, hydrogel-bottomed microwell arrays. Several material properties of these films, including optical characteristics, surface chemistry, and permeability are analyzed. Finally, the application of these hybrid films to studies of cellular heterogeneity is described. Platforms co-fabricated from chitosan and epoxy photoresist can be used to reduce both high-molecular weight biochemical crosstalk between cells and mixing of different clonal populations, and will enable high-throughput cellular studies with increased ability to customize dynamic interrogations when compared to the materials in currently available technologies.

2. Materials and methods

2.1 Materials

Chitosan (medium molecular weight), γ-Butyrolactone (GBL), photoresist developer (propylene glycol methyl ether acetate, PGMEA), toluidine blue, FITC-dextrans (average molecular weights 4, 10, 20, 40, and 70 kDa), rhodamine B-dextran (70 kDa), glutaraldehyde (70% v/v), and mineral oil were purchased from Sigma-Aldrich (St. Louis, MO). EPON resin 1002F photoresist was obtained from Miller-Stephenson (Sylmar, CA). UVI-6976 photoinitiator (triarylsulfonium hexafluoroantimonate salts in propylene carbonate) was purchased from Dow Chemical (Torrance, CA). Polydimethylsiloxane (PDMS) was obtained from Dow Corning (Midland, MI). Chrome photolithography masks were designed using TurboCAD software and printed by FineLine Imaging (Boulder, CO). RPMI 1640 medium, fetal bovine serum (FBS), penicillin/streptomycin, Dylight 488-NHS ester, and tetramethylrhodamine-conjugated BSA were obtained from Life Technologies (Grand Island, NY). Ba/F3 cells carrying the BCR-Abl fusion gene were a kind gift from Dr. Brian Druker at Oregon Health Sciences University. Transwell™ polystyrene cassettes were obtained from Corning Life Sciences (Tewksbury MA).

2.2 Co-fabrication of freestanding 1002F:chitosan films

Chitosan was dissolved in 0.5% (w/w) acetic acid to a concentration of 2% (w/w). Dry films of chitosan were obtained by spin coating dissolved chitosan at 2000 rpm onto pre-cleaned, air plasma oxidized glass slides and baking at 95°C for 1 h. Micropatterned films of 1002F negative photoresist were fabricated atop the dry chitosan films following a 2-min air plasma treatment as described previously [17]. Briefly, EPON resin 1002F negative photoresist, dissolved in GBL and mixed with UVI-6076 photoinitiator, was spin-coated atop the dry chitosan films to a desired thickness of 40-50 μm and soft-baked at 95°C to remove organic solvent. After exposure to UV light through a patterned chrome photomask, the hybrid film was given a post-exposure bake, first at 95°C and then at 120°C, and then developed in PGMEA to remove unpolymerized photoresist. The resulting micropatterned hybrid film was hard-baked to solidify the photoresist layer. After affixing a polystyrene cassette pre-cut with a hollow center 12 mm in diameter using a PDMS mortar, the chitosan layer was neutralized and the hybrid film released via incubation in 0.1% (w/w) aqueous NaOH for 48 h. Precise process conditions for hybrid films with a photoresist layer ∼50 μm thick are otherwise identical to those previously reported [17]. Immediately after release, the

hybrid films were gently washed with deionized water and the chitosan hydrogel layer was immersed in phosphate buffered saline (PBS) pH 7.4 for at least 12 h before use.

2.3 Imaging

Critical point-dried hybrid films were imaged using an FEI Quanta 200 FEG scanning electron microscope (SEM), operated at 0.38 torr (Chapel Hill Analytical and Nanofabrication Laboratory (CHANL)). High-resolution images of the chitosan layer at the bottom of microwells in critical point-dried hybrid films were obtained using a Hitachi S-4700 Cold Cathode Field Emission scanning electron microscope (CHANL).

A Nikon Eclipse TE2000-U inverted fluorescence microscope, controlled by NIS Elements software (Nikon, Melville, NY), was used to image films for optical property measurements, during diffusion and protein conjugation experiments, and for daily cellular analyses. Time-lapse live-cell imaging was accomplished using an IX-81 inverted microscope (Olympus, Center Valley, PA) equipped with an MS-2000 robotic *xy* stage (Applied Scientific Instrumentation, Eugene, OR). All brightfield and fluorescence micrographs were recorded with a cooled CCD camera (Photometrix Cool Snap fx, Roper Scientific, Tucson, AZ). Fluorescence micrographs were analyzed using Image J (NIH, Bethesda, MD).

2.4 Measurement of 1002F:chitosan film optical properties

Glass coverslips were deposited into a multiwall polystyrene plate, and background absorbance spectra from 300-800 nm were obtained using a SpectraMax M5 microplate reader (Molecular Devices, Sunnyvale, CA). Dry films of chitosan were prepared above the same coverslips by spin-coating chitosan at 500 rpm and baking for 1 h at 95°C. The films were then neutralized in 0.1% (w/w) NaOH for 30 min and rehydrated in 1× PBS at pH 7.4 for 1 h. Chitosan absorbance was obtained by measuring absorbance for the spin-coated coverslips and subtracting out the background absorbance of the coverslip alone. Results from six replicates were averaged to give an absorbance spectrum.

The fluorescence of chitosan was measured and compared to that of glass coverslips and to the negative photoresists 1002F and SU-8. Chitosan, 1002F, and SU-8 were spin coated at 2000 rpm onto clean glass coverslips and baked to remove solvent, after which the chitosan was neutralized by immersion into 0.1% (w/w) NaOH and blown dry with nitrogen gas, while the 1002F- or SU-8-coated coverslips were exposed to UV light without a photomask, post-exposure baked, developed, and hard-baked as described above. Films were imaged via fluorescence microscopy using UV (ex 340-380 nm / em 435-485 nm), GFP (ex 465-495 nm / em 515-555 nm), Texas Red (ex 522-592 nm / em 584-664 nm), and Cy5 (ex 588-668 nm / em 652-732 nm) Nikon filter sets. Fluorescence of the chitosan and photoresist layers in each wavelength set was quntified using ImageJ to calculate the mean pixel intensity for each material. Clean glass coverslips not spin-coated with any material were measured in parallel. Three spin-coated slides were measured for each of the three materials listed, as well as for the glass blanks. Two regions per slide were analyzed.

2.5 Covalent protein conjugation

1002F:chitosan hybrid films and glass-bottomed 1002F through-hole arrays, each micropatterned with 100-μm diameter wells, were fabricated, affixed to polystyrene cassettes as described above, treated with an air plasma for 2 min, immersed in PBS, and imaged to obtain background fluorescence micrographs. Films were patterned with protein via a covalent coupling strategy using the homobifunctional crosslinker glutaraldehyde. Glutaraldehyde was prepared as a 4% (v/v) solution in PBS, after which 500 μL was deposited atop each of the films named above and incubated for 4 h at room temperature. Films supplied with PBS only served as controls. After removing glutaraldehyde solution and washing five times with PBS, activated films were imaged to measure autofluorescence and then incubated with 250 μL of BSA-tetramethylrhodamine (0.1 mg/mL) for 2 h at room temperature in the dark. After aspirating away the protein solution and washing five times with PBS, films were imaged via fluorescence microscopy. Fluorescence within the microwell spaces and atop the microwell walls was quantified using Image J to analyze fluorescence micrographs. Three films were used for each experimental group.

2.6 Measurement of diffusion

1002F:chitosan hybrid films micropatterned with 900 wells (100-μm diameter) were fabricated, affixed to 12-mm diameter polystyrene cassettes, plasma oxidized for 2 min, and released as described above. The films where then placed into a 12-well plate, suspended by the cassette approximately 1 mm from the well bottom. PBS was supplied into the cassette (upper) and the dish (lower) compartments at volumes (0.5 and 1.5 mL, respectively) recommended by the plate manufacturer to give an equal height between the two compartments. Either toluidine blue dye (MW 270 Da), Dylight 488-glucosamine conjugate (MW 1074 Da), or one of several FITC-dextrans (average molecular weights 4, 10, 20, and 40 kDa) was supplied into the upper fluid compartment as bolus solutions in PBS to a final concentration of either 0.01% (w/w)(toluidine blue), 10 μM (Dylight 488-glucosamine), or 200 μg/mL (FITC-dextrans). Dylight 488-glucosamine conjugate was prepared in-house by reacting 10 mg/mL of Dylight 488-NHS ester dissolved in anhydrous DMF with a 10 mM solution of glucosamine dissolved in PBS. Rhodamine B-conjugate dextran (70 kDa) at a concentration of 200 μg/mL was supplied as a high-MW, slow-transit negative control across the several experiments. Plates were covered to prevent evaporation, and incubated at room temperature. At regular time points, 60 and 15 μL samples were taken from the bottom and top (respectively) fluid compartments for analysis using a SpectraMax M5 microplate reader (Molecular Devices, Sunnyvale, CA). Seven different devices, representing four different fabrication batches of films, were tested in this manner. Commercially-available track-etch membranes with pores 400 nm in diameter (Corning Life Sciences, Tewksbury MA) were used as positive controls for dye diffusion. Toluidine blue concentrations were measured via absorbance at 633 nm, while Dylight 488-glucosamine conjugate and FITC-dextran concentrations were measured via fluorescence (ex 490 nm / em 520 nm). Rhodamine B-dextran fluorescence was also measured (ex 545 nm / em 580 nm) for each sample.

Calculation of the diffusion constant (also known as the diffusivity) was achieved by modeling the plate wells in which the 1002F:chitosan hybrid films were incubated during

each diffusion experiment as a closed, two-compartment system, separated by a membrane of fixed thickness *h* and permeable area A in a manner similar to a model described by Lee *et al.* [48]. Volumes of each compartment are based on the volumes of fluid supplied to them at the initiation of the diffusion experiment. The source compartment initial concentration is the concentration of dye supplied to it, while the initial concentration of the sink compartment is assumed to be zero. Theoretical equilibrium concentration (C_{eq}) for each hybrid film tested was defined to be the mean steady-state dye concentration in the bottom compartment of the positive diffusion controls. The value of *h* is the thickness of the chitosan layer. Diffusivities for each of the solutes studied were calculated through a linearization scheme according to the model[48].

2.7 Expansion of nonadherent cells entrapped in medium micropockets

Ba/F3 cells carrying the BCR-Abl fusion gene were maintained in RPMI 1640 medium supplemented with penicillin/streptomycin and 10% fetal bovine serum. 1002F:chitosan hybrid films micropatterned with 900 wells (100-μm diameter) were fabricated, affixed to 12 mm-diameter polystyrene cassettes, and released as described above. After a 2 min plasma oxidation and ethanol sterilization, films were placed into 12-well plates filled in the bottom compartments with RPMI 1640 medium. Ba/F3 cells were deposited into the cassette compartment at a density of 2.0×10^4 cells / cm^2 in 500 μL of media. After 20 min, microarrays were inspected via brightfield microscopy to confirm that cells had settled into the chitosan-bottomed microwells, at which point the media in the upper compartment was carefully aspirated away and 350 μL of filter-sterilized mineral oil was overlaid in order to trap the cells in medium droplets in the microwells. Cells were also seeded at the same density into two additional sets of chitosan-bottomed microwell arrays fabricated with a design identical to that described above but not released from the glass fabrication surface (so as to yield dead-ended microwells). After cell seeding and removal of the cell seeding media, one array set was gently refilled with culture medium, while a second array set was overlaid with 250 μL of sterile mineral oil. All arrays were imaged daily with brightfield microscopy to assess cell morphology and proliferation.

2.8 Time-lapse video imaging of nonadherent cell proliferation

Ba/F3 BCR-Abl cells were centrifuged and resuspended in serum-free RPMI 1640 medium and incubated for 12 h, after which cells were again centrifuged and then resuspended in RPMI growth medium with serum. Cells were then seeded into the cassette compartment of 1002F:chitosan hybrid films fabricated as described in the above paragraph at a density of 2.0×10^4 cells / cm^2, allowed to settle, and confined to microwells using a mineral oil overlay. Two films were placed into a single 12-well plate, and the plate was transferred into a sealed live imaging microscopy enclosure, custom-built and maintained at 37°C with 60% humidity and 5% CO_2. Both microwell arrays (total 1800 microwells) were imaged every 15 min for a period of 60 h. The final number of cells present in each well that began the experiment with a single cell was manually counted using the resulting micrographs, and the times at which cell division occurred were noted for five microwells representative of the range of final cell number; these cell division times were used to construct a lineage tracing for each representative cell.

2.9 Statistical testing

Unless otherwise stated, all statistical analyses performed utilized the student t-test. Statistical significance was defined as $p < 0.05$.

3. Results and Discussion

3.1 Co-fabrication of freestanding 1002F:chitosan films

Freestanding 1002F:chitosan hybrid films were fabricated and micropatterned using the strategy depicted in Fig. 1A and described in detail in the Methods section. Briefly, dry chitosan films were prepared on glass by spin coating and baking. After an air-plasma treatment, 1002F photoresist was spin-coated atop the dry chitosan films and micropatterned via UV photolithography. The resulting hybrid films, featuring an array of microwells patterned into the 1002F film and bottomed by a layer of chitosan, were plasma-treated and released from the glass substrate by incubation in dilute NaOH. By affixing a polystyrene cassette and placing into a 6- or 12-well plate the films adopted a setup similar to commercially available Transwell™ permeable supports, in which a membrane (here, the chitosan layer) separates two compartments (Fig. 1B): an “upper” compartment that interfaced with the photoresist film and the microwells patterned into it, and the “lower” compartment that lay beneath the chitosan layer.

Scanning electron micrographs of the resulting released hybrid films, shown in Fig. 2A-B, confirm that the thin chitosan layer formed a bottom to the microwells patterned from the photoresist layer. The chitosan layer, as shown in Fig. 2C, was revealed to be a uniform film approximately 400 nm thick composed of entangled chitosan polysaccharide chains with tortuous pores of irregular shape and diameters on the order of tens of nanometers. Fig. 2D reveals the chitosan layer to have a pebbled, irregular surface, again showing pores of irregular shape and diameters on the order of tens of nanometers. While tears can form in the chitosan layer during the release process, this was nearly always found to occur in cases in which the incubation in dilute NaOH was less than 48 h.

Chitosan proved to be a useful material due to the ability to adjust its solubility by varying the pH of the solution. By employing an acidic medium, chitosan could be made soluble, after which its concentration could be adjusted to yield a solution viscous enough for spin-coating. Using profilometry, the thickness of dry films spin-coated at various speeds was measured. The thickness of the dry films ranged from 179-799 nm (Fig. S1, Table S1) suggesting that chitosan layers of variable height can be achieved (for such considerations as mechanical strength) simply by varying the spin coating speed. Additional formulations using higher or lower concentrations of chitosan would be expected to give thicker or thinner films, respectively, based on identical spin-coat speeds.

These results demonstrated that the thickness of a dry chitosan film fabricated by spin coating at the speed typically used in the co-fabrication protocol (2000 rpm) was 349 ± 24 nm (n=3). Comparison of this thickness to that measured by SEM (see Figure 2C) reveals that released and rehydrated films are 13% thicker than dry films. This increase in thickness is likely due to slight osmotic swelling of the chitosan hydrogel layer that occurs in a pH-dependent manner [49].

3.2 Optical properties

Because brightfield and especially fluorescence microscopy is anticipated to be a chief means of analyzing cells cultured using the 1002F:chitosan hybrid films, the absorption and autofluorescence of chitosan films, fabricated in a similar fashion to those described above, were measured. Absorbance spectra of glass coverslips spin coated with chitosan films 800 nm thick, shown in Fig. 3A, revealed an absorbance below 0.02 (≥95.5% transmittance) at wavelengths above 400 nm. Because these films were thicker by a factor of ∼2 than chitosan layers in typically fabricated 1002F:chitosan hybrid films, absorbances of chitosan layers fabricated with the typical protocol are likely to be even less.

The fluorescence of films of typical fabrication thickness was measured for chitosan (800 nm), 1002F (45 μm thick), or SU-8 (45 μm thick). Chitosan films exhibited very low autofluorescence and the chitosan film fluorescence was comparable to that of a glass coverslip (Fig. 3B). In contrast, both 1002F and especially SU-8 photoresists demonstrated considerable fluorescence particularly in the blue wavelengths. While there were significant differences in thickness between the chitosan and photoresist layers tested, the thickness of each layer reflects a typical thickness used for microfabrication and so provides a useful comparison. Overall, the low absorption and autofluorescence of chitosan across the visible wavelengths suggested that applications employing both qualitative and quantitative microscopy for cellular analysis will be compatible with 1002F:chitosan hybrid films.

3.3 Spatially controlled protein conjugation

The free amine group in the molecular structure of chitosan has been used in numerous applications for conjugating exogenous molecules to chitosan surfaces [20, 44-45]. However, the reactivity between amines and epoxides (a reactive group found in 1002F photoresist) is well-documented, suggesting the possibility that chitosan at the surface of the microwell bottoms was devoid of free, unbound amines. To investigate this, x-ray photoelectron spectroscopy (XPS) was used to examine dry chitosan surfaces that had been co-fabricated and patterned with 1002F. Qualitative and quantitative analysis of x-ray photoelectron spectra revealed that, in terms of the locations and areas of C 1s and N 1s spectral peaks and the thickness of the surface molecular layer [50], the chitosan surfaces co-fabricated and patterned with 1002F and subsequently treated with an air plasma exhibited notable differences from identical surfaces that had not received an air plasma treatment, but only negligible differences from films of native chitosan (Fig. S2, Table S2). Together, these results suggest that while the fabrication steps do result in bonding between free amines from surface-level chitosan and overlying 1002F, the post-fabrication plasma oxidation and neutralization steps typically employed in this protocol lead to the removal of this layer, leaving chitosan with free amines at the surface of the microwell bottoms.

Having verified that the free amine group is preserved in the chitosan layer bottoming the microwells, the potential to utilize the amine group to achieve material-specific and spatially controlled molecular patterning was explored. Chitosan:1002F films with 100-μm diameter wells were patterned with tetramethylrhodamine-conjugated BSA via a covalent coupling strategy using the homobifunctional crosslinker glutaraldehyde (Fig. 4A). As shown in Fig. 4B, films activated with glutaraldehyde exhibited a fold increase of 14.9 ± 1.9 in average

fluorescence within the microwells when compared to baseline ($p < 0.003$), and a 1.9 ± 0.2 fold increase over films lacking glutaraldehyde activation before incubation with labeled protein ($p = 0.03$), suggesting that activation of the chitosan surface resulted in higher deposition of protein onto the microwell bottoms as compared to protein adsorption onto the same surface. However, in 1002F microwells fabricated atop a glass substrate and thus lacking chitosan, fluorescence within the microwells failed to increase in a statistically significant manner (1.2 ± 0.3 fold, treated, vs. 1.5 ± 0.3 fold, untreated), suggesting that the fluorescence increase observed with glutaraldehyde treatment is specific to the chitosan surface. Fluorescence micrographs showing the effect of glutaraldehyde treatment are shown in Fig. 4C.

Previous work has demonstrated the ability to label chitosan films through their full thickness with amine-reactive NHS-fluorescein [51]. We hypothesize that either the length of incubation time in this experiment or the network pore size of the chitosan layer was insufficient for the labeled BSA (larger than NHS-fluorescein) to infiltrate past the top few microns of the chitosan layer and would explain why only the chitosan surface within the microwells appeared to be labeled. This covalent conjugation scheme can likely be adapted to utilize other crosslinkers or amine-reactive silanes in order to allow user-defined and spatially-controlled surface functionalizations that are selective for the chitosan layer at the bottom of the microwells.

3.4 Measurement of solute diffusion across micropatterned 1002F: chitosan hybrid films

In order to determine whether solutes could diffuse across the chitosan layer at the bottom of the microwells in the 1002F:chitosan films, the permeability of the chitosan layer to small-molecule solute diffusion was first measured. A general diffusion scheme is depicted in Fig. 5A, in which freestanding chitosan:1002F hybrid films affixed to polystyrene cassettes were placed in a 12-well plate and PBS was supplied to the upper and lower compartments. Addition of a bolus of concentrated dye to the upper compartment created a gradient to drive solute diffusion from the “source” compartment, across the chitosan membrane, and into the lower “sink” compartment.

Toluidine blue dye (MW 270 Da) seeded into the upper compartment was visually observed to enter and disperse throughout the lower compartment (Fig. S3A). By 48 h, the dye concentration in the lower compartment had reached 90.8 ± 3.2% of its maximal value and 88.9 ± 1.3% of the concentration in the top compartment, compared with 90.9 ± 0.9% and 98.2 ± 13.4% (respectively) for unpatterned Transwell™ membranes used as positive controls. Fig. S3B illustrates the time course of absolute toluidine blue concentration in the lower compartment for 1002F:chitosan membranes and the positive controls. These data suggest that the chitosan membranes have comparable permeability to small molecules as membranes with cylindrical track-etch micropores, indicating that the chitosan hydrogel layer remained permeable to small molecules after the fabrication process was completed. Employing this same method with a high-MW FITC-conjugated dextran (MW 70 kDa) instead of toluidine blue dye, however, revealed that after 48 h of incubation, the concentration of solute in the bottom compartment was only 0.2 ± 0.1% of that in the top compartment, compared to a value of 31.6 ± 2.2% for a positive control (data not shown).

Given the possibility that the chitosan layer had a molecular exclusion limit, diffusion of solutes in a range of molecular weights was investigated. Using the method described above, diffusion of FITC-conjugated dextrans of molecular weights 4, 10, 20, and 40 kDa were investigated. Fig. 5B shows the concentration of each dextran, relative to its theoretical equilibrium concentration C_{eq}, over the course of time. Dextrans with molecular weights 4 and 10 kDa were shown to diffuse through chitosan membranes, reaching half-theoretical maximum values by 48 and 120 h, respectively (Fig. 5B). Compared to those dextrans, diffusion of dextran with MW 20 kDa was greatly reduced, reaching C / C_{eq} value of only 0.2 after 5 days of incubation, and dextran with MW 40 kDa did not exhibit appreciable diffusion at all, similar to earlier data that FITC-dextran with a higher MW of 70 kDa exhibited no detectable diffusion across the membrane. In all samples except the positive controls, diffusion of 70 kDa rhodamine B-conjugated dextran was not observed, consistent with earlier results.

To determine the frequency and effect of any defects in the chitosan layer on solute diffusion, a method (described in Supplementary Materials) was devised to track and measure molecular diffusion in individual wells in an ensemble fashion. Data generated in this fashion, shown in Fig. S4, revealed that less than 0.1% of microwells exhibited permeability to 40 kDa FITC-dextran, the molecular weight shown above to exhibit negligible diffusion across chitosan:1002F films. This suggests that defects in the chitosan layer did not occur with sufficient frequency so as to explain the observed movement of dye from the top compartment into the bottom. Diffusion data generated in this fashion (Fig. S4) reveal permeability of the chitosan layer to 10 and 20 kDa FITC-dextran and exclusion of 40 kDa dextran, consistent with data presented above.

Using a mathematical model based on Fick's First Law and reported by Lee *et al*. [48], the diffusion coefficient, D, through the chitosan membrane was calculated for solutes of varying molecular weight (Fig. 5C). D ranged in order of magnitude from 10^{-9} to 10^{-12} cm^2 / s (Table 1) and fall within the range of previously reported values for slow solute diffusion within a solid [52]. Lower molecular weight solutes predictably had higher diffusion coefficients, and 40 kDa dextran was found to have a diffusivity a full order of magnitude less than that of 20 kDa dextran.

Analysis of the linear range of these data indicated that the theoretical molecular exclusion limit (the molecular weight at which the linear extrapolated diffusivity is zero) was 9.9 ± 2.1 kDa for the chitosan membrane in the 1002F:chitosan hybrid films. This value and range is in agreement with the observed diffusion of 10 kDa-MW FITC-dextran and with the failure to observe diffusion of 40- and 70 kDa MW dextrans through the membrane. Because the calculated molecular exclusion limit is a theoretical value based on a linear extrapolation, solutes with molecular weights higher than the theoretical cutoff can still exhibit measurable diffusion, a case also found in the data of Lee *et al.* [48] and with the slow (though quantifiable) diffusion of 20-kDa FITC-dextran in our experiments.

This theoretical molecular exclusion limit, and the failure to observe diffusion of dextrans > 40 kDa, differs from other reports describing the size of pores in chitosan microparticles or capsules as being 10 μm or higher [21, 37], and from data suggesting that antibodies (MW

150 kDa) can permeate through chitosan membranes fabricated *in situ* on a microfluidic device [46]. However, the processing conditions under which the chitosan membrane was formed in these other reports differ greatly from those reported here, in which chitosan membranes were prepared as dry films prior to photoresist spin coating and UV photolithography. It is hypothesized that the fabrication steps employed here, especially the baking steps necessary for proper polymerization of the photoresist, lead to a high degree of chitosan entanglement and possibly thermal crosslinking that reduce the network pore size and therefore lower the molecular exclusion size limit. Two early reports describing permeability through chitosan films that had been dried noted the exclusion of solutes with molecular weights above 13 kDa, while permitting passage of solutes 2.9 kDa and lighter, supporting the findings described here [53-54].

Previous reports describe the fabrication of microscale wells over a track-etched permeable membrane [55-56]. However, the co-fabrication of chitosan with 1002F as reported here presents certain advantages, including: (1) the use of spin-coating to achieve control over both the membrane thickness and the microwell depth; (2) the use of UV photolithography to directly fabricate microwell features, avoiding the risk of undercutting as might be found in a molding-based technique; and (3) the potential to tailor the membrane permeability by crosslinking or adjustment of chitosan entanglement. Additionally, there were no observed instances of delamination between the chitosan film and the 1002F layer, presumably due to covalent bonding between amine groups in the chitosan and epoxide moieties in the 1002F that served to anchor the chitosan to the 1002F layer. Polymer membranes that have been track-etched with cylindrical micropores to make them permeable are commercially available (*e.g.* the Transwell systems). However these track-etched membranes possess micropores that are generally at least 400 nm in diameter and which are therefore permeable to extremely large molecules.

3.5 Survival and proliferation of nonadherent cells entrapped in chitosan-bottomed microwells

Microwells fabricated using the most common methods and materials in use in the microfabrication field – namely soft lithography using polydimethylsiloxane (PDMS), photolithography using photoresists, and injection molding using cyclic olefin co-polymer – result in impermeable supports for subsequent growth of cells [57-60]. While certain techniques, such as overlaying a physical barrier onto microwells seeded with cells, can reduce biochemical crosstalk and intermixing of clonal populations, cell survival and viability can be compromised over the long term as cells consume the small quantities of culture media with which they are seeded [16]. As a consequence, maintenance of cells beyond several hours necessitates that cells be exposed to a relatively large media reservoir that can allow biochemical crosstalk and the intermixing of clonal cell populations, confounding subsequent inquiries.

Having established that the chitosan layer at the bottom of the 1002F microwells was permeable to solutes up to 20 kDa, we hypothesized that a microdevice such as the one depicted in Fig. 6A, would enable physical isolation of clonal cell populations without a loss of cell viability. By supplying culture medium to the compartment below the permeable

chitosan film, nutrients and metabolites could be exchanged across the chitosan membrane and proliferating cells could be maintained within each microwell. In order to ensure that cell survival and proliferation was not affected by the chitosan or 1002F material properties, Ba/F3 cells were cultured on polystyrene, glass, chitosan films, or 1002F films and the cell number counted over time. The number of cells on the surfaces was not statistically different after 96 h of culture (Fig. S5) suggesting that proximity to the chitosan or 1002F did not impact cell growth.

To formally demonstrate the utility of this platform in physically isolating micropopulations of cells and preventing mixing of the cells between microwells (45 μm depth), Ba/F3 cells were seeded onto released hybrid platforms and isolated via oil overlay. Expansion of cells was compared to cells seeded onto control microwell arrays that were not released from the underlying glass support (yielding dead-ended microwells). In one control, cells were seeded, after which the media was aspirated and cells were overlaid with mineral oil; in the second control, cells were seeded, media removed, and the chamber was refilled with fresh media. The first (oil-overlay) control exhibited no clonal expansion of cells (presumably due to either rapid depletion of nutrients from the ~400-pL microwell volume or poor delivery of oxygen) (Fig. 6B, top row). This was in sharp contrast to the second control, in which clonal expansion was observed. However, with this control, numerous wells empty after the initial cell seeding were noted to have cells present in them by 48 hours (Fig. 6B, middle row). These results indicate that cell migration and mixing of clonal populations was occurring in this control sample. Deeper wells (100 μm depth) did not eliminate cell movement between microwells (data not shown). Arrays of 1002F:chitosan microwells supplied with media *via* the bottom compartment and overlaid with oil, also exhibited heterogeneous clonal expansion (Fig. 6B, bottom row), but showed no migration of cells into microwells that were empty after the initial cell seeding. Repeating this experiment but supplying the bottom compartment with serum-negative media, however, resulted in a failure of cells to proliferate (Fig. S6). This observation establishes that the cell proliferation observed with the freestanding films was due to serum growth factors present in the media supplied to the bottom compartment and not growth factors present in the seeding media. Thus the chitosan membranes were functionally permeable to the serum growth factors necessary for proliferation of the cells. Altogether, these results confirm the hypothesis that this platform could be used to clonally expand cells but keep different clonal populations separate, all the while permitting each of those subpopulations to be interrogated *en masse*.

Serum contains a number of very high molecular weight entities required by cells which might have been the proximate cause of the cell-growth failure in the prior experiment. To show targeted blockage of a single protein of a relatively low molecular weight (39 kDa), murine colonoids or colon-derived organoids were cultured on the arrays. Wnt is required for the maintenance of stem/progenitor cells in these organoids. In the absence of Wnt, all cells rapidly differentiate into nondividing, terminal cell types. Colonoids originally derived from mice expressing DsRED under a chicken actin promoter and eGFP under a Sox9 promoter were cultured on the chitosan-bottomed arrays. In these colonoids, DsRED is expressed in all cells while eGFP is expressed only in stem/transit amplifying cells. Media with all required constituents except Wnt was added to the upper and lower fluid

compartments of the arrays (Fig S7A,B). When Wnt-3A was added to the upper compartment, the colonoids grew robustly and displayed both DsRED and eGFP fluorescence at day 3 of culture suggesting the presence of stem/transit amplifying cells (Fig S7C). Colonoids grown with Wnt placed below the chitosan film grew poorly and did not possess eGFP fluorescence indicating an absence of stem/transit amplifying cells (Fig S7D). These data demonstrate that the transit of Wnt-3a (39 kDa) into the microwells with colonoids was effectively blocked by the chitosan film.

3.6 Analysis of cell division heterogeneity in entrapped, nonadherent cells

In trials of cellular entrapment and survival, it was observed that the rate of cell proliferation was very heterogeneous amongst cells seeded onto the microwell array, as shown in Fig. 7A. To assay the extent of cellular heterogeneity in a single population of cells, the proliferation of Ba/F3 cells was observed for cells in 47 separate microwells. Fig. 7B shows that the average number of cells per well increased to 1.6 ± 0.6 at 24 h, 2.3 ± 1.1 at 48 h, and finally to 5.2 ± 4.2 at 72 h for wells initially seeded with a single cell. Cells in wells with 2 cells initially expanded to 3.2 ± 0.9, 4.9 ± 2.3, and 11.1 ± 6.5 cells by 24, 48, and 72 h respectively. The high variability in the number of cells per well, especially by day 3 in culture, suggested that some cells were proliferating faster than others, generating greater numbers of daughter clone cells. Mean cell doubling times were determined to be 31.4 ± 3.9 and 29.8 ± 3.4 hours for wells with 1 and 2 cells per well after initial seeding, respectively. For comparison, the mean doubling time for cells grown in dead-ended microwells (20.4 ± 4.7 h) with a media overlay was shorter suggesting that diffusional movement of larger sized molecules across the membrane might impact cell growth rates in these ultra-small volume microwells. Alternatively optimization of oil biocompatibility may lessen this doubling time difference.

Suspecting that there was a large range of doubling times in the oil-overlaid, chitosanbottomed wells, a relative frequency histogram of cell doubling time was constructed (relative frequency referring to the ratio of the number of cells whose doubling times fell in the indicated range to the total number of cells observed). Fig. 7C shows that cell doubling time ranged from just over 18 to greater than 80 h, with mean and median doubling times of 40.1 and 32.8 h, respectively. While 36% of cells had doubling times between 25 and 41 h (*i.e.* there were not two wholly separate populations of “fast” and “slow” dividers that drove the average to a middle value), the presence of *some* apparent fast and slow dividers (doubling times < 22 and >60 h) was appreciated. Of note, cells could be maintained at least to 96 h, but beyond 72 h the number of cells in certain wells was sufficiently large that an accurate cell count could not be established. It is expected that by adjusting fabrication parameters to yield wells with larger diameters, accurate cell counts beyond 72 h would be possible.

To achieve a more precise description of the heterogeneity of proliferation rates in this population of cells, time-lapse video imaging of cell proliferation on the microwell array was undertaken. After serum-starvation to synchronize cell cycles, cells were seeded into microwells and entrapped with mineral oil as described above. After supply of media with serum to the bottom compartment, the array was placed into a humidified and temperature-

controlled cabinet for automated live-cell imaging. Microwells with two or more initial cells were excluded from this analysis. Table 2 indicates the frequency with which a range of final cell numbers was observed for 256 microwells that began with a single cell. Lineage tracings of five cells, representative of this range of survival outcomes and proliferation rates, are shown in Fig. 7D.

These results provide further evidence of the growing importance of heterogeneity among the various cells in a biological system, a theme with applications in such fields as cancer biology, immunology, stem cell biology and regenerative medicine [61-68]. While a number of methods are currently available for analyzing cellular heterogeneity, limitations in each method exist [11, 69-70]. Flow cytometry is a widely-used approach that can generate a large amount of data, but is limited to a single interrogation time, and can also provide confounded data, resulting from changes in cell physiology due to the stressful nature of the flow cytometer apparatus [71-74]. Certain high-throughput technologies, such as microtiter plates and even high-throughput format Transwell® systems, can be used to assay a large number of cells, but do not allow the ability to discriminate between different clonal cell populations unless limiting dilution steps are employed to seed only and precisely one cell per plate well. Droplet microfluidic systems are similarly high-throughput, but long-term culture of cells in droplets is difficult due to issues with reduced oxygen and nutrient delivery, as well as the need to preload droplets with analytical reagents [10-12]. While droplets with an encapsulating semi-permeable film can be generated using a double-emulsion technique, our method allows for the observation and storage of cells in encapsulated, fixed medium pockets that can be tracked over time, a feature not available to droplet-based devices without even more specialized equipment [75]. One recent report that specifically examined the range of doubling times in a population of hematopoietic stem cells utilized a microfluidic device featuring nanoliter-scale growth chambers, but media exchange is dependent on a series of microvalves [76]. PEG-DA hydrogels have been used previously in microwell fabrications via a microstamping method, in which the PEG-DA forms both the semi-permeable membrane and the well walls [77]. However, the use of PEG-DA as a material for the well walls would fail to abrogate biochemical crosstalk between microwells, since secreted factors could diffuse through the walls themselves, even if an oil overlay was used to physically confine cells to the microwells. In these regards, PEG-DA would prove less advantageous when compared with impermeable 1002F.

When compared with the technologies named above for analyzing cellular heterogeneity, the 1002F:chitosan hybrid platform described here holds numerous advantages. The materials used in this platform are commercially available, biocompatible, and well-characterized. The fabrication process is rapid and allows easy tailoring of the platform's features. Cellular analyses conducted using the hybrid films require no other specialty equipment, namely continuous perfusion or droplet-generating devices, for growing cells after the devices are fabricated. Additionally and without the need for microscale valves to achieve correct fluid flow, this setup features the ability to rapidly exchange media and reagents from around the cells without risk of mixing of clonal subpopulations. This feature will allow users to customize the order and timeframe of reagent delivery and removal. Adherent cells were also readily cultured on the chitosan-bottomed arrays (Fig. S8).

4. Conclusions

This microfabricated cellular analysis platform will enable high-throughput study of cellular heterogeneity in response to user-defined and dynamically controlled stimulations. This platform features an array of microscale wells, formed via the co-fabrication of chitosan with an epoxy photoresist to form a freestanding array of microwells bound by a semi-permeable hydrogel layer. Through a variety of methods, we have described numerous material properties of this biocompatible hybrid platform. More importantly, an overlaid layer of inert mineral oil above the wells allows cells lying in the wells to be physically isolated from other wells, reducing confounding cellular migration and biochemical crosstalk, while maintaining chemical access to the cells for exchange of nutrients and small molecules supplied by the user. Use of this platform will enable future high-throughput studies of the diversity in cellular biochemistry and genetics.

Supplementary Material

Refer to Web version on PubMed Central for supplementary material.

Acknowledgments

The authors are grateful to Ms. Lauren Westerhold for fabrication assistance and Mr. Joseph Balowski for helpful discussions, as well as to Dr. Carrie Donley (CHANL) for expertise with XPS analysis and Dr. Wallace Ambrose (CHANL) for SEM imaging assistance. This work was supported by a grant from the National Institutes of Health (CA177993).

References

1. Kovarik ML, Gach PC, Ornoff DM, Wang Y, Balowski J, Farrag L, et al. Micro total analysis systems for cell biology and biochemical assays. Anal Chem. 2012; 84:516–40. [PubMed: 21967743]
2. Park JY, Takayama S, Lee SH. Regulating microenvironmental stimuli for stem cells and cancer cells using microsystems. Integr Biol. 2010; 2:229–40.
3. Nikkhah M, Edalat F, Manoucheri S, Khademhosseini A. Engineering microscale topographies to control the cell-substrate interface. Biomaterials. 2012; 33:5230–46. [PubMed: 22521491]
4. Wong IY, Bhatia SN, Toner M. Nanotechnology: emerging tools for biology and medicine. Genes Dev. 2013; 27:2397–408. [PubMed: 24240230]
5. Kovarik ML, Ornoff DM, Melvin AT, Dobes NC, Wang Y, Dickinson AJ, et al. Micro total analysis systems: fundamental advances and applications in the laboratory, clinic, and field. Anal Chem. 2013; 85:451–72. [PubMed: 23140554]
6. Voldman J, Gray ML, Schmidt MA. Microfabrication in biology and medicine. Annual review of biomedical engineering. 1999; 1:401–25.
7. Li N, Tourovskaia A, Folch A. Biology on a chip: microfabrication for studying the behavior of cultured cells. Crit Rev Biomed Eng. 2003; 31:423–88. [PubMed: 15139302]
8. Shim J, Bersano-Begey TF, Zhu X, Tkaczyk AH, Linderman JJ, Takayama S. Micro- and nanotechnologies for studying cellular function. Current topics in medicinal chemistry. 2003; 3:687–703. [PubMed: 12570859]
9. Yarmush ML, King KR. Living-cell microarrays. Annual review of biomedical engineering. 2009; 11:235–57.
10. Joensson HN, Andersson Svahn H. Droplet microfluidics--a tool for single-cell analysis. Angew Chem Int Ed Engl. 2012; 51:12176–92. [PubMed: 23180509]
11. Love KR, Bagh S, Choi J, Love JC. Microtools for single-cell analysis in biopharmaceutical development and manufacturing. Trends in Biotechnology. 2013; 31:280–6. [PubMed: 23582471]

12. Guo MT, Rotem A, Heyman JA, Weitz DA. Droplet microfluidics for high-throughput biological assays. Lab Chip. 2012; 12:2146–55. [PubMed: 22318506]
13. Love JC, Ronan JL, Grotenbreg GM, van der Veen AG, Ploegh HL. A microengraving method for rapid selection of single cells producing antigen-specific antibodies. Nat Biotechnol. 2006; 24:703–7. [PubMed: 16699501]
14. Wang Y, Sims CE, Marc P, Bachman M, Li GP, Allbritton NL. Micropatterning of Living Cells on a Heterogeneously Wetted Surface. Langmuir. 2006; 22:8257–8262. [PubMed: 16952271]
15. Wang Y, Phillips C, Xu W, Pai JH, Dhopeshwarkar R, Sims CE, et al. Micromolded arrays for separation of adherent cells. Lab Chip. 2010; 10:2917–24. [PubMed: 20838672]
16. Lindstrom S, Andersson-Svahn H. Single-cell culture in microwells. Methods in Molecular Biology. 2012; 853:41–52. [PubMed: 22323139]
17. Ornoff DM, Wang Y, Allbritton NL. Characterization of freestanding photoresist films for biological and MEMS applications. J Micromech Microeng. 2013; 23:025009. [PubMed: 24072957]
18. Muzzarelli RAA, Muzzarelli C. Chitosan chemistry: Relevance to the biomedical sciences. Adv Polym Sci. 2005; 186:151–209.
19. Kumar MNVR, Muzzarelli RAA, Muzzarelli C, Sashiwa H, Domb AJ. Chitosan chemistry and pharmaceutical perspectives. Chem Rev. 2004; 104:6017–6084. [PubMed: 15584695]
20. Koev ST, Dykstra PH, Luo X, Rubloff GW, Bentley WE, Payne GF, et al. Chitosan: an integrative biomaterial for lab-on-a-chip devices. Lab Chip. 2010; 10:3026–3042. [PubMed: 20877781]
21. Madihally SV, Matthew HWT. Porous chitosan scaffolds for tissue engineering. Biomaterials. 1999; 20:1133–1142. [PubMed: 10382829]
22. Nunthanid J, Puttipipatkhachorn S, Yamamoto K, Peck GE. Physical properties and molecular behavior of chitosan films. Drug Dev Ind Pharm. 2001; 27:143–157. [PubMed: 11266226]
23. Niamsa N, Baimark Y. Preparation and characterization of highly flexible chitosan films for use as food packaging. American Journal of Food Technology. 2009; 4:162–169.
24. Lu GY, Kong LJ, Sheng BY, Wang G, Gong YD, Zhang XF. Degradation of covalently cross-linked carboxymethyl chitosan and its potential application for peripheral nerve regeneration. Eur Polym J. 2007; 43:3807–3818.
25. He Q, Ao Q, Gong YD, Zhang XF. Preparation of chitosan films using different neutralizing solutions to improve endothelial cell compatibility. J Mater Sci-Mater M. 2011; 22:2791–2802. [PubMed: 22042456]
26. Srinivasa PC, Ramesh MN, Tharanathan RN. Effect of plasticizers and fatty acids on mechanical and permeability characteristics of chitosan films. Food Hydrocolloid. 2007; 21:1113–1122.
27. Tomihata K, Ikada Y. In vitro and in vivo degradation of films of chitin and its deacetylated derivatives. Biomaterials. 1997; 18:567–575. [PubMed: 9105597]
28. Mi FL, Tan YC, Liang HF, Sung HW. In vivo biocompatibility and degradability of a novel injectable-chitosan-based implant. Biomaterials. 2002; 23:181–191. [PubMed: 11762837]
29. Berthod F, Saintigny G, Chretien F, Hayek D, Collombel C, Damour O. Optimization of Thickness, Pore-Size and Mechanical-Properties of a Biomaterial Designed for Deep Burn Coverage. Clin Mater. 1994; 15:259–265. [PubMed: 10147169]
30. Chatelet C, Damour O, Domard A. Influence of the degree of acetylation on some biological properties of chitosan films. Biomaterials. 2001; 22:261–268. [PubMed: 11197501]
31. Zheng H, Du YM, Yu JH, Xiao L. The properties and preparation of crosslinked chitosan films. Chem J Chinese U. 2000; 21:809–812.
32. Cao WL, Cheng MY, Ao Q, Gong YD, Zhao NM, Zhang XF. Physical, mechanical and degradation properties, and Schwann cell affinity of cross-linked chitosan films. J Biomat Sci-Polym E. 2005; 16:791–807.
33. Chung TW, Lu YF, Wang SS, Lin YS, Chu SH. Growth of human endothelial cells on photochemically grafted Gly-Arg-Gly-Asp (GRGD) chitosans. Biomaterials. 2002; 23:4803–9. [PubMed: 12361619]

34. Amaral IF, Unger RE, Fuchs S, Mendonca AM, Sousa SR, Barbosa MA, et al. Fibronectin-mediated endothelialisation of chitosan porous matrices. Biomaterials. 2009; 30:5465–75. [PubMed: 19615736]
35. Chu XH, Shi XL, Feng ZQ, Gu ZZ, Ding YT. Chitosan nanofiber scaffold enhances hepatocyte adhesion and function. Biotechnol Lett. 2009; 31:347–52. [PubMed: 19037598]
36. Ao Q, Wang A, Cao W, Zhang L, Kong L, He Q, et al. Manufacture of multimicrotubule chitosan nerve conduits with novel molds and characterization in vitro. J Biomed Mater Res A. 2006; 77:11–8. [PubMed: 16345091]
37. Di Martino A, Sittinger M, Risbud MV. Chitosan: a versatile biopolymer for orthopaedic tissue-engineering. Biomaterials. 2005; 26:5983–90. [PubMed: 15894370]
38. Obara K, Ishihara M, Ishizuka T, Fujita M, Ozeki Y, Maehara T, et al. Photocrosslinkable chitosan hydrogel containing fibroblast growth factor-2 stimulates wound healing in healing-impaired db/db mice. Biomaterials. 2003; 24:3437–44. [PubMed: 12809772]
39. Shu XZ, Zhu KJ, Song WH. Novel pH-sensitive citrate cross-linked chitosan film for drug controlled release. Int J Pharm. 2001; 212:19–28. [PubMed: 11165817]
40. Karlsen J, Skaugrud O. Excipient Properties of Chitosan. Manuf Chemist. 1991; 62:18–19.
41. Sawayanagi Y, Nambu N, Nagai T. Permeation of Drugs through Chitosan Membranes. Chem Pharm Bull (Tokyo). 1982; 30:3297–3301.
42. Kanke M, Katayama H, Tsuzuki S, Kuramoto H. Appilcation of Chitin and Chitosan to Pharmaceutical Preparations. I. : Film Preparation and in Vitro Evaluation. Chem Pharm Bull (Tokyo). 1989; 37:523–525.
43. Bonvin MM, Bertorello MM. In vitro sodium salicylate release from chitosan films. Polymer Bulletin. 1993; 31:375–379.
44. Yi H, Wu LQ, Bentley WE, Ghodssi R, Rubloff GW, Culver JN, et al. Biofabrication with chitosan. Biomacromolecules. 2005; 6:2881–94. [PubMed: 16283704]
45. Cheng Y, Luo X, Payne GF, Rubloff GW. Biofabrication: programmable assembly of polysaccharide hydrogels in microfluidics as biocompatible scaffolds. Journal of Materials Chemistry. 2012; 22:7659–7666.
46. Luo X, Berlin DL, Betz J, Payne GF, Bentley WE, Rubloff GW. In situ generation of pH gradients in microfluidic devices for biofabrication of freestanding, semi-permeable chitosan membranes. Lab Chip. 2010; 10:59–65. [PubMed: 20024051]
47. Luo X, Wu HC, Tsao CY, Cheng Y, Betz J, Payne GF, et al. Biofabrication of stratified biofilm mimics for observation and control of bacterial signaling. Biomaterials. 2012; 33:5136–43. [PubMed: 22507453]
48. Lee CJ, Vroom JA, Fishman HA, Bent SF. Determination of human lens capsule permeability and its feasibility as a replacement for Bruch's membrane. Biomaterials. 2006; 27:1670–1678. [PubMed: 16199085]
49. Lowman, A.; Peppas, N. Hydrogels. In: Mathiowitz, E., editor. Encyclopedia of Controlled Drug Delivery. Wiley-Interscience; 1999.
50. Cumpson PJ, Seah MP. Elastic Scattering Corrections in AES and XPS. II. Estimating Attenuation Lengths and Conditions Required for their Valid Use in Overlayer/Substrate Experiments. Surface and Interface Analysis. 1997; 25:430–446.
51. Wu LQ, Yi HM, Li S, Rubloff GW, Bentley WE, Ghodssi R, et al. Spatially selective deposition of a reactive polysaccharide layer onto a patterned template. Langmuir. 2003; 19:519–524.
52. Deen, WM. Analysis of transport phenomena. Oxford University Press; New York: 1998. p. xix, 597
53. Hirano S, Tobetto K, Hasegawa M, Matsuda N. Permeability properties of gels and membranes derived from chitosan. J Biomed Mater Res. 1980; 14:477–85. [PubMed: 6156945]
54. Hirano S, Tobetto K, Noishiki Y. SEM ultrastructure studies of N-acyl- and N-benzylidene-chitosan and chitosan membranes. J Biomed Mater Res. 1981; 15:903–11. [PubMed: 7309771]
55. Torisawa YS, Mosadegh B, Cavnar SP, Ho M, Takayama S. Transwells with Microstamped Membranes Produce Micropatterned Two-Dimensional and Three-Dimensional Co-Cultures. Tissue Eng Part C Methods. 2010

56. Paz AC, Javaherian S, McGuigan AP. Tools for micropatterning epithelial cells into microcolonies on transwell filter substrates. Lab Chip. 2011; 11:3440–8. [PubMed: 21860858]
57. Ratner BD, Bryant SJ. Biomaterials: where we have been and where we are going. Annual review of biomedical engineering. 2004; 6:41–75.
58. Zorlutuna P, Annabi N, Camci-Unal G, Nikkhah M, Cha JM, Nichol JW, et al. Microfabricated biomaterials for engineering 3D tissues. Adv Mater. 2012; 24:1782–804. [PubMed: 22410857]
59. Whitesides GM, Ostuni E, Takayama S, Jiang X, Ingber DE. Soft lithography in biology and biochemistry. Annual review of biomedical engineering. 2001; 3:335–73.
60. Gates BD, Xu Q, Stewart M, Ryan D, Willson CG, Whitesides GM. New approaches to nanofabrication: molding, printing, and other techniques. Chem Rev. 2005; 105:1171–96. [PubMed: 15826012]
61. Walling MA, Shepard JR. Cellular heterogeneity and live cell arrays. Chem Soc Rev. 2011; 40:4049–76. [PubMed: 21487572]
62. Meacham CE, Morrison SJ. Tumour heterogeneity and cancer cell plasticity. Nature. 2013; 501:328–37. [PubMed: 24048065]
63. Almendro V, Marusyk A, Polyak K. Cellular heterogeneity and molecular evolution in cancer. Annu Rev Pathol. 2013; 8:277–302. [PubMed: 23092187]
64. Chung CH, Bernard PS, Perou CM. Molecular portraits and the family tree of cancer. Nat Genet. 2002; 32(Suppl 1):533–40. [PubMed: 12454650]
65. Ghoreschi K, Laurence A, Yang XP, Hirahara K, O'Shea JJ. T helper 17 cell heterogeneity and pathogenicity in autoimmune disease. Trends Immunol. 2011; 32:395–401. [PubMed: 21782512]
66. Taylor JJ, Jenkins MK, Pape KA. Heterogeneity in the differentiation and function of memory B cells. Trends Immunol. 2012; 33:590–7. [PubMed: 22920843]
67. Narsinh KH, Sun N, Sanchez-Freire V, Lee AS, Almeida P, Hu S, et al. Single cell transcriptional profiling reveals heterogeneity of human induced pluripotent stem cells. J Clin Invest. 2011; 121:1217–21. [PubMed: 21317531]
68. Cahan P, Daley GQ. Origins and implications of pluripotent stem cell variability and heterogeneity. Nat Rev Mol Cell Biol. 2013; 14:357–68. [PubMed: 23673969]
69. Smith C. Cancer biology: Cancer shows strength through diversity. Nature. 2013; 499:505–508. [PubMed: 23887432]
70. Barteneva NS, Ketman K, Fasler-Kan E, Potashnikova D, Vorobjev IA. Cell sorting in cancer research--diminishing degree of cell heterogeneity. Biochim Biophys Acta. 2013; 1836:105–22. [PubMed: 23481260]
71. Piercy KT, Donnell RL, Kirkpatrick SS, Mundy BL, Stevens SL, Freeman MB, et al. Effect of harvesting and sorting on beta-1 integrin in canine microvascular cells. J Surg Res. 2001; 100:211–6. [PubMed: 11592795]
72. Seidl J, Knuechel R, Kunz-Schughart LA. Evaluation of membrane physiology following fluorescence activated or magnetic cell separation. Cytometry. 1999; 36:102–11. [PubMed: 10554157]
73. Grossmann J. Molecular mechanisms of “detachment-induced apoptosis--Anoikis”. Apoptosis. 2002; 7:247–60. [PubMed: 11997669]
74. Reddig PJ, Juliano RL. Clinging to life: cell to matrix adhesion and cell survival. Cancer Metastasis Rev. 2005; 24:425–39. [PubMed: 16258730]
75. Chan HF, Zhang Y, Ho YP, Chiu YL, Jung Y, Leong KW. Rapid formation of multicellular spheroids in double-emulsion droplets with controllable microenvironment. Sci Rep. 2013; 3:3462. [PubMed: 24322507]
76. Lecault V, Vaninsberghe M, Sekulovic S, Knapp DJ, Wohrer S, Bowden W, et al. High-throughput analysis of single hematopoietic stem cell proliferation in microfluidic cell culture arrays. Nat Methods. 2011; 8:581–6. [PubMed: 21602799]
77. Kobel SA, Lutolf MP. Fabrication of PEG hydrogel microwell arrays for high-throughput single stem cell culture and analysis. Methods in molecular biology. 2012; 811:101–12. [PubMed: 22042675]

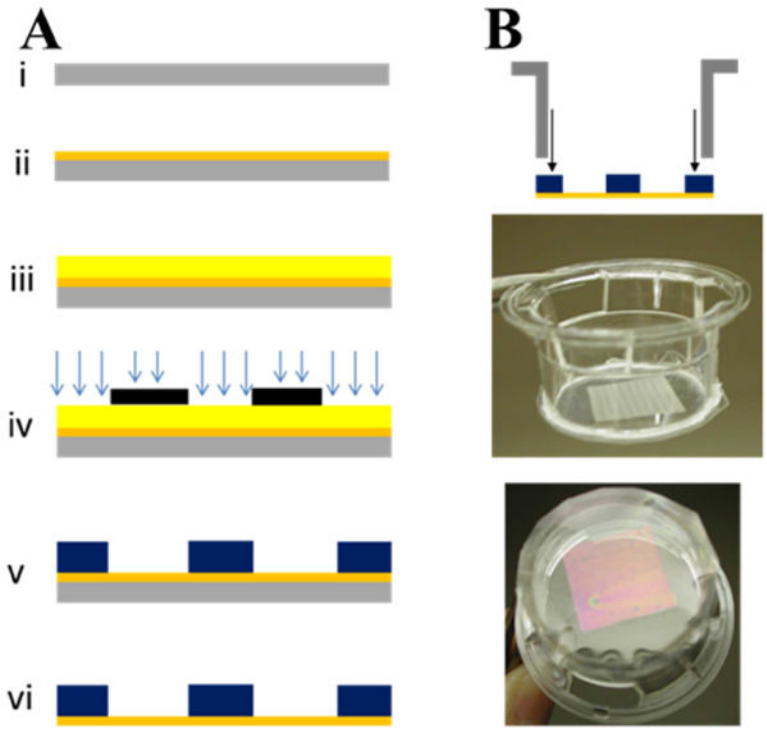

Fig. 1.

Fabrication and release of chitosan hydrogel-bottomed microwell array films. (A) Fabrication and release protocol. Atop a clean glass slide (i), the chitosan layer is deposited via spin-coating and then baked (ii). 1002F negative photoresist is then spin-coated atop chitosan layer and soft-baked (iii). UV exposure through a patterned photomask (iv) and subsequent development yields a microwell array bottomed by a layer of chitosan (v). Soaking in dilute NaOH allows hydration of the chitosan layer and release from the glass substrate, yielding a freestanding chitosan: 1002F hybrid film (vi). (B) Attachment of a polystyrene cassette to the film creates a two-compartment cell culture system. The upper and lower compartments are separated by the chitosan hydrogel layer (note the purple sheen of the submicron chitosan layer).

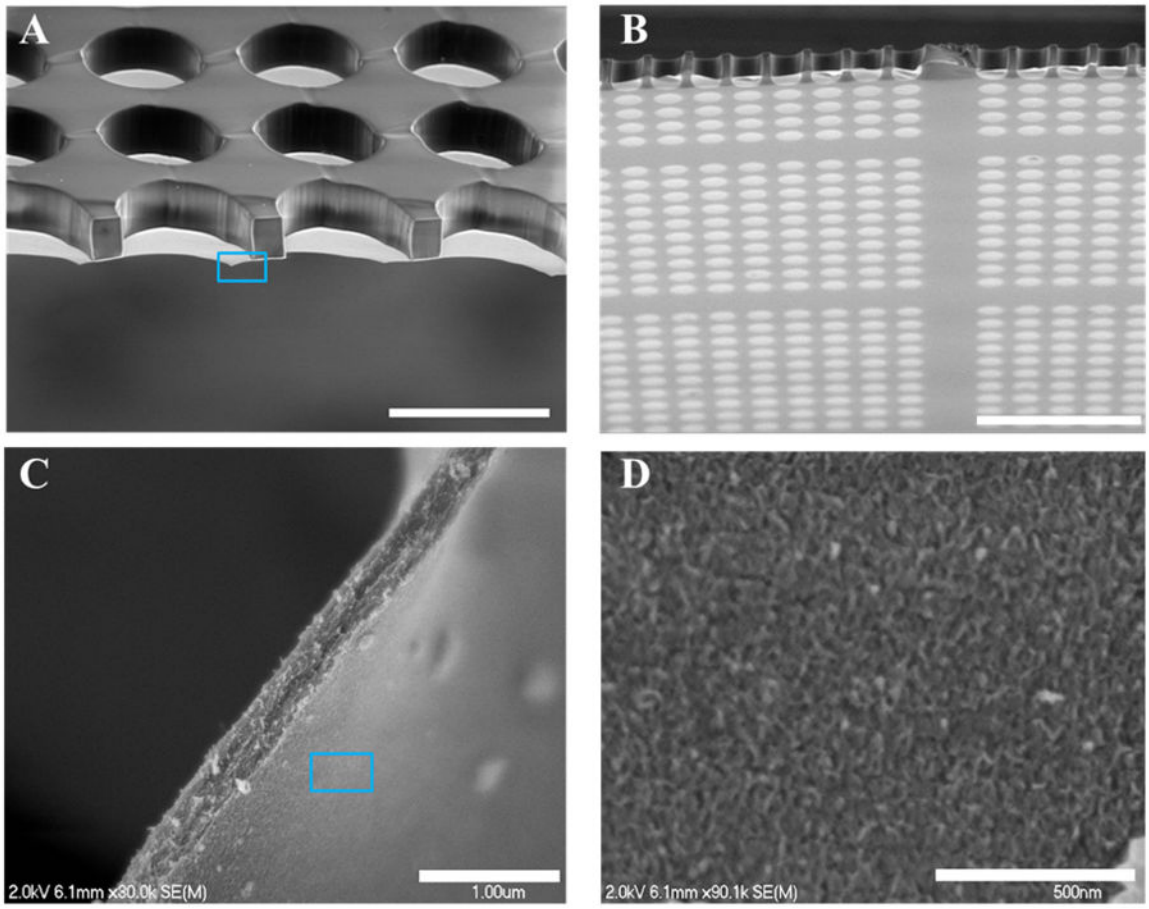

Fig. 2.

Imaging of released chitosan-bottomed microwell array films. (A-B) Scanning electron micrographs of released, freestanding 1002F:chitosan films imaged from above (A) and below (B) the 1002F layer. Each film features 75 μm-diameter microwells 45 μm deep. (C-D) Scanning electron micrograph of chitosan hydrogel layer cross-section (C) and surface (D). (C) shows the area marked by the blue box in (A), while (D) shows the area marked by the blue box in (C). Scale bars: (A) 100 μm; (B) 400 μm; (C) 1 μm; (D) 500 nm.

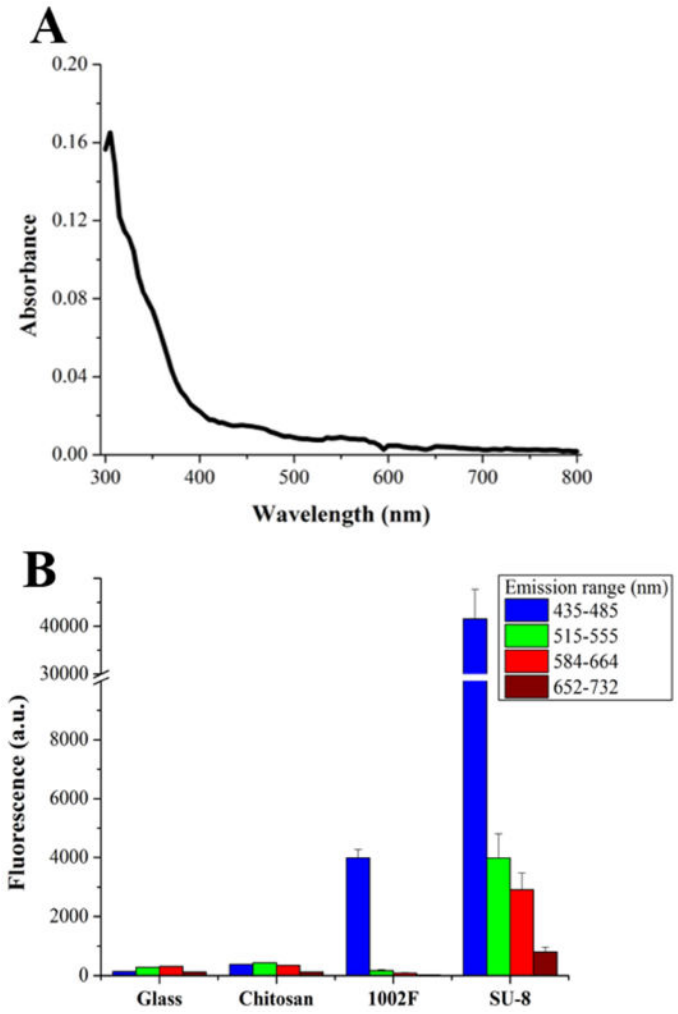

Fig. 3.

Optical properties of chitosan films. (A) Absorbance spectrum of hydrated chitosan films 800 nm in thickness. Spectrum is based on mean absorbance from n = 6 films. (B) Autofluorescence of a glass coverslip or chitosan, 1002F, and SU-8 in co-fabricated films. Data presented are as mean ± SD, n ≥ 3 films each.

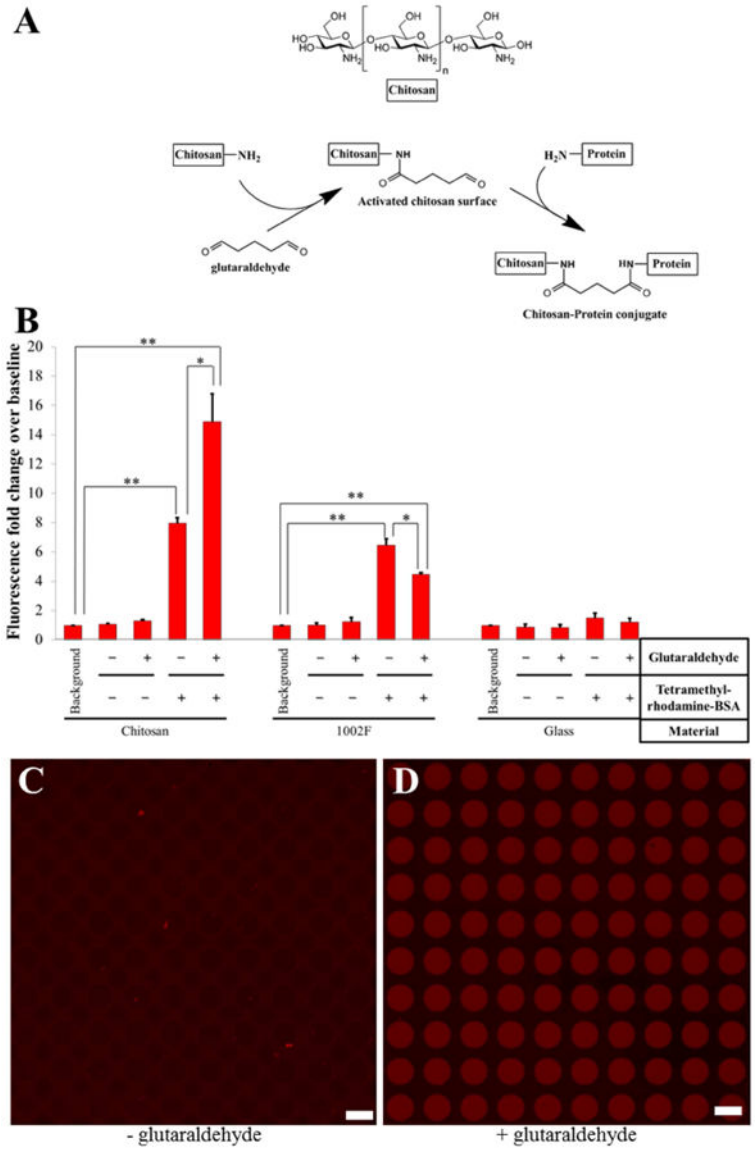

Fig. 4.

Spatially-selective covalent modification of chitosan surfaces. (A) Covalent conjugation scheme. Use of the homobifunctional crosslinker glutaraldehyde allows functionalization of the chitosan surface via its amine moiety for covalent attachment of macromolecules with free amines. (B) Quantification of fluorescence fold change over baseline of chitosan- or glass-bottomed 1002F microwell arrays incubated with BSA-tetramethylrhodamine after treatment with either PBS or glutaraldehyde. * $p < 0.05$, ** $p < 0.01$, n = 3 films each. (C-D) Fluorescence micrographs of chitosan-bottomed 1002F microwell arrays incubated with BSA-tetramethylrhodamine after treatment with either PBS (C) or glutaraldehyde (D). Scale bars: 100 μm.

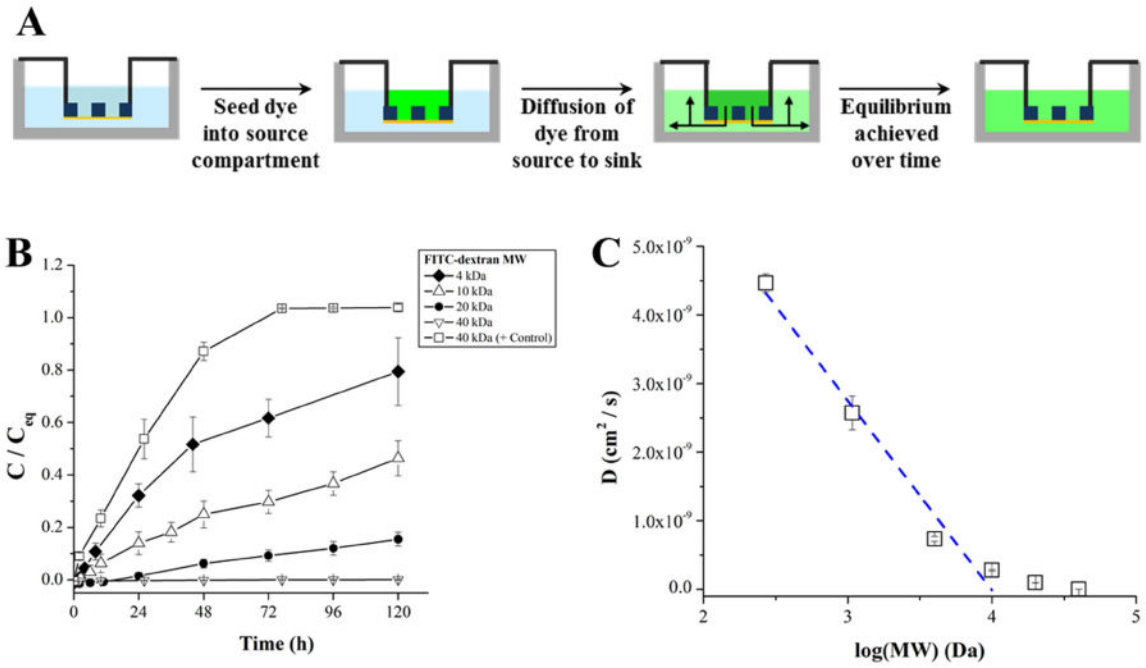

Fig. 5.

Permeability of micropatterned 1002F:chitosan films. (A) Workflow diagram for testing solute diffusion through chitosan-bottomed microwell arrays. After seeding concentrated dye into the upper compartment of freestanding micropatterned films, dye solute will diffuse across the chitosan layer and into the bottom compartment. Samples are taken at regular intervals from each compartment to determine solute concentration in the compartments. (B) Quantitation of the ratio of FITC-dextran concentration C to its theoretical equilibrium value C_{eq} for four different molecular weights of dextran diffusing across a chitosan-bottomed 1002F microwell array. Data are presented as mean ± SD for each time point, n = 7 films. (C) Determination of the theoretical molecular exclusion limit of chitosan films in the 1002F:chitosan hybrid devices via extrapolation in a plot of diffusivity vs log(MW). The theoretical molecular weight exclusion limit is the extrapolated x-intercept of a line fitted to the linear region of the D vs log (MW) plot.

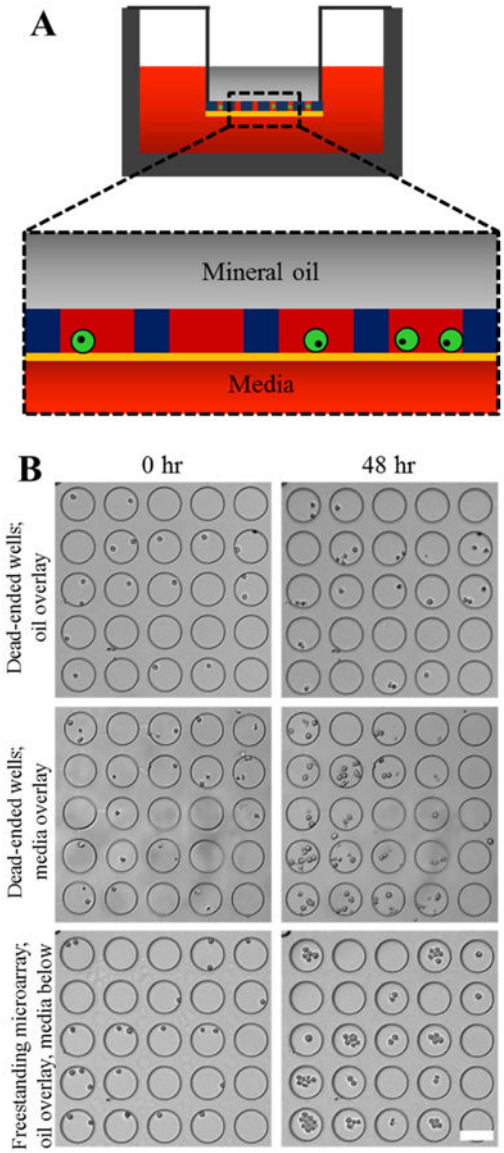

Fig. 6.

Entrapment of highly proliferative, non-adherent cells in culture medium micropockets. (A) Design schematic for entrapping and maintaining nonadherent cells within micropockets of culture medium. Seeding cells into chitosan-bottomed microwells and aspirating excess media off discontinuously de-wets the upper compartment. Overlay of mineral oil entraps cells in the microwells. (B) Physical isolation of clonal cell populations in microwell medium pockets. Cells were seeded into unreleased (dead-ended, top two rows) or released (freestanding, bottom row) 1002F:chitosan microwell arrays and imaged daily over 48 hours. Dead-ended microwell arrays were either overlaid with mineral oil or culture medium, while freestanding microwell arrays were overlaid with mineral oil in the upper compartment and supplied with culture medium was supplied to the bottom compartment. Scale bar (lower right): 100 μm.

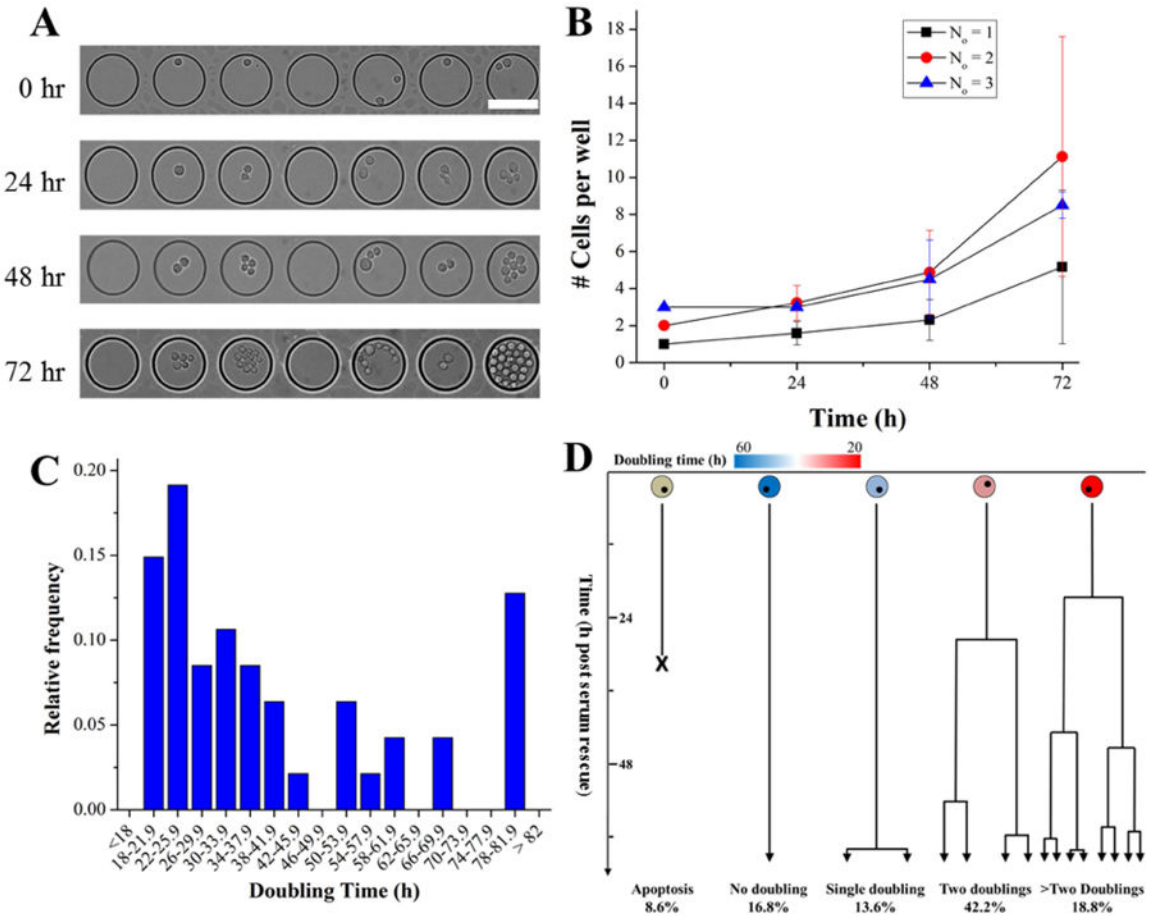

Fig. 7.

Quantitation and heterogeneity of cell proliferation in isolated microwell medium pockets. (A) Several adjacent microwells illustrate the heterogeneity of cell proliferation within a bulk population of cells. (B) Measurement of number of cells per microwell over time, stratified by the initial number of cells in each microwell. Data are shown as mean ± SD for 256 microwells. (C) Relative frequency distribution of cell doubling time, calculated and aggregated based on number of cells present within a given microwell, was determined for 256 separate microwells. (D) Time-lapse imaging analysis of single cells in 256 microwells permits lineage tracing of clonally-expanding individual cells. Lineage tracing of 5 cells representative of the heterogeneity in proliferation rates is shown.

Table 1

Comparison of diffusivity constants to solute molecular weight for chitosan membranes in 1002F:chitosan hybrid films.

MW (Da)	log MW	D (cm^2 / s)	Error in D
270	2.431364	4.46×10^{-9}	1.32×10^{-10}
1074	3.031004	2.57×10^{-9}	2.44×10^{-10}
4000	3.60206	7.36×10^{-10}	3.54×10^{-11}
10000	4	2.81×10^{-10}	1.02×10^{-11}
20000	4.30103	9.68×10^{-11}	2.27×10^{-12}
40000	4.60206	3.42×10^{-12}	1.36×10^{-13}

Table 2

Distribution of final cell number from clonally expanding single cells clonally expanding in chitosan-bottomed 1002F microwells. n = 256 microwells, each with a single cell.

Final number of cells	Percentage of microwells
0 (apoptosis)	8.6%
1	16.8%
2	13.7%
3	7.8%
4	34.4%
5	5.1%
6	6.6%
7	3.5%
8	2.3%
9	0.0%
10	0.4%
11	0.4%
12	0.4%